Experimental Observation of Single Skyrmion Signatures in a Magnetic Tunnel Junction

N. E. Penthorn, ¹ X. Hao, ² Z. Wang, ² Y. Huai, ² and H. W. Jiang ^{1,*}

¹Department of Physics and Astronomy, University of California, Los Angeles, California 90095, USA

²Avalanche Technology, Fremont, California 95438, USA

(Received 10 December 2018; published 26 June 2019)

We have deterministically created a stable topological spin texture in magnetic tunnel junctions (MTJ) by using pulsed or microwave currents. The spin texture is characterized by a field-dependent intermediate resistance state and a new magnetic resonance. Micromagnetic simulations show that the observations are consistent with the nucleation of a single skyrmion, facilitated by a spatially nonuniform stray field. The unique resonance spectrum is identified as the skyrmion breathing mode and a skyrmion diameter of 75 nm is estimated. This work shows the possibility to create skyrmions in MTJs without the Dzyaloshinskii-Moriya interaction and could lead to noninvasive, on-chip skyrmion measurement.

DOI: 10.1103/PhysRevLett.122.257201

Research on magnetic skyrmions, localized topological spin textures in magnetic materials, has gained momentum in recent years due to the technological advancement of magnetic films and the possible application of skyrmions in information storage and processing. For memory applications, much experimental attention has been given to the racetrack architecture where skyrmions are shuttled along a thin magnetic film with an applied current [1]. Moreover, there have been computational studies demonstrating the use of skyrmions for logic gates [2], artificial synapses for neuromorphic computing [3], and harboring Majorana bound states for topological quantum computing [4]. Because of low creation energy, robustness to defects and compact size, magnetic skyrmions have considerable potential in the field of spintronics.

The majority of experimental research has been restricted to multi-skyrmion states in thin magnetic films, but there is substantial interest in device settings where individual skyrmions need to be generated and read out on chip. A popular design solution for electrical creation and detection of skyrmions is the magnetic tunnel junction (MTJ) [5,6], as MTJs are arguably the most promising spintronics devices developed in recent years for data storage, sensing, and logic computation. Tunnel magnetoresistance (TMR) is an excellent way to sensitively measure the magnetization of an MTJ's constituent magnetic layers, and the writing energy required to create or annihilate a magnetic skyrmion in the free layer of an MTJ has been predicted to be at least 1 order of magnitude less than that of state-of-the-art spin transfer torque (STT)-based memory architectures, at room temperature and with no bias fields or currents [7]. Despite the promise of high-speed, lowenergy skyrmion creation and detection, there is currently no experimental evidence of skyrmions in MTJs.

One particular challenge in realizing skyrmions in MTJs is the development of unconventional detection methods.

The prevailing technique to identify skyrmion states is to directly image the magnetic configuration of the device of interest via electron or x-ray microscopy, ptychography, and magnetic force microscopy [8,9,10]. While imaging techniques give unambiguous measurements of skyrmion size and evolution, they require the magnetic layer to be exposed to a certain extent, which changes the MTJ free layer magnetic properties and limits their utility for onchip, electrically excited skyrmion devices. Another challenge in the MTJ approach to skyrmion creation is engineering the magnetic environment necessary to induce transitions from the ferromagnetic state to a skyrmionic state in the MTJ free layer, while maintaining the requisite layer structure in the MTJ to allow for high TMR and electrical manipulation of the free layer magnetization. Normally, this may be accomplished by introducing a sufficiently strong interfacial Dzyaloshinskii-Moriya interaction (DMI) to stabilize the spin texture [11,12]. However, there is strong evidence that skyrmions can be stabilized in a confined ferromagnetic environment without the need of DMI [13,14]. Notably, a time-resolved study of currentinduced switching in MTJs found that a transient magnetic bubble state is sometimes nucleated during switching and can persist for microseconds before thermal annihilation [15]. If thermal effects are suppressed, however, it is reasonable to expect that a single skyrmion can be sustained in the MTJ free layer once it is created by current-induced spin-transfer torque or voltage-controlled magnetic anisotropy [16,17].

In this Letter we show evidence that conditions for skyrmion creation inside a commercially available MTJ can be met at suitably low temperatures, and we demonstrate the electrical creation and detection of a stable nonuniform state with concurrent measurements of a MTJ's steady-state magnetoresistance and spin-polarized current-induced ferromagnetic resonance. Simulations show that the

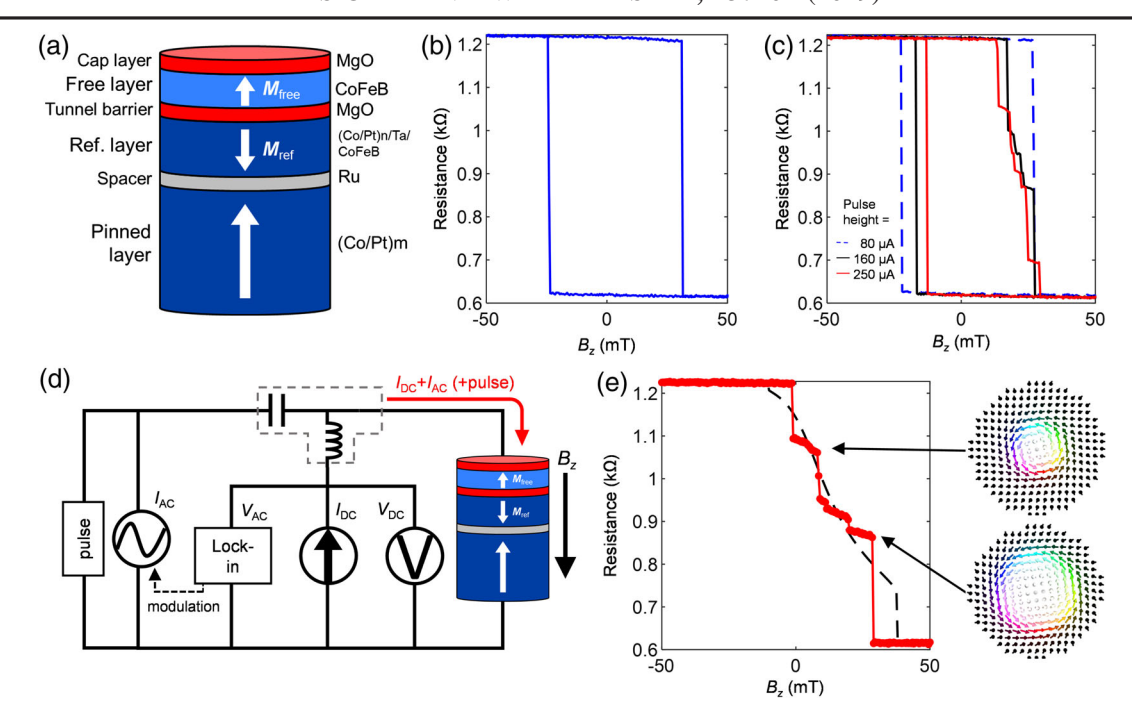


FIG. 1. (a) MTJ layer structure. Arrows denote average magnetization of each layer at zero applied field. The positive z direction is taken to be parallel to the reference layer magnetization. (b) Out-of-plane hysteresis loop in the absence of pulsed or microwave current excitation, showing a completely perpendicular free layer magnetization. (c) Out-of-plane hysteresis loop in the presence of a repeated pulse of width 10 ns. A transition to an intermediate resistance state (IRS) appears when the pulse height exceeds 100 μ A. The P \rightarrow AP switching field is reduced due to the presence of spin torques. (d) Circuit diagram for magnetoresistance measurements. (e) Magnetic field dependence of the IRS with no applied excitations following initialization at 24 mT (red line) and comparison to simulations of a single skyrmion (dotted black line). Right side: snapshots of the stable skyrmion configuration at 5 (upper) and 15 mT (lower).

characteristics of this state are consistent with single skyrmion creation. We find that the electrically detected skyrmion breathing mode [18] in the resonance spectrum provides a noninvasive means for on-chip skyrmion identification.

The MTJ samples were prepared using Avalanche standard MRAM processes [19]. The magnetic layer stack was deposited using PVD and etched into nanopillars with diameters ranging from 80 to 400 nm. For this study we focus on three MTJs with 250, 350, and 400 nm diameters that all displayed qualitatively similar behavior. The MTJ layer stack and experimental setup are shown in Figs. 1(a) and 1(d). The MTJs are composed of a CoFeB-based free layer, an MgO tunneling barrier and an out-of-plane pinned synthetic antiferromagnet reference layer [24,25]. Additionally, there is a thin MgO capping layer on top of the free layer. Cryogenic testing was performed in a Janis sorption-pumped ³He refrigerator.

Figure 1(b) shows a typical out-of-plane hysteresis loop of the magnetoresistance of a 250 nm MTJ in the absence of pulsed or microwave current excitation. The free layer is found to have out-of-plane magnetization at 4.2 K due to perpendicular magnetic anisotropy (PMA) induced by the MgO/CoFeB interface [26], characterized by a rectangular hysteresis loop as function of magnetic field B_z with sharp transitions between ferromagnetic states. This loop shows

the expected parallel (P) -to-antiparallel (AP) switching characteristics that are common for MTJ structures. An unexpected observation is made when a current pulse train, with a pulse width of 10 ns and a repetition rate of 100 kHz, is superimposed onto the small dc bias current. Instead of the sharp AP \rightarrow P transition, an intermediate resistance state (IRS) region emerges. The width of the IRS region is a function of pulse height and it reaches 30 mT at large pulse heights. Once created, this new state persists even when the pulse is off. However, ferromagnetism is recovered when the applied field is stronger than the coercive field B_c (about 30 mT). It is important to note that the IRS is not observed for the P \rightarrow AP transition.

We find that the IRS can also be deterministically created when a continuous microwave current $I_{\rm ac}$ is applied at selected range of frequencies $f_{\rm drive}$. As shown in Fig. 2(b), the IRS is observed in the hysteresis loop for 1.3 and 1.7 GHz, for a 350 nm MTJ. When the frequency is fixed and the microwave power is decreased, the switching field gets closer to B_c and the IRS region diminishes [Fig. 2(c)]. Figure 2(a) displays a phase diagram of the IRS as a function of $f_{\rm drive}$ and B_z . These results are reminiscent of the well-studied microwave-assisted switching in MTJs and spin valves, where the microwave current-induced STT promotes domain nucleation in the free layer and reduces the switching energy [27]. Microwave-assisted switching is

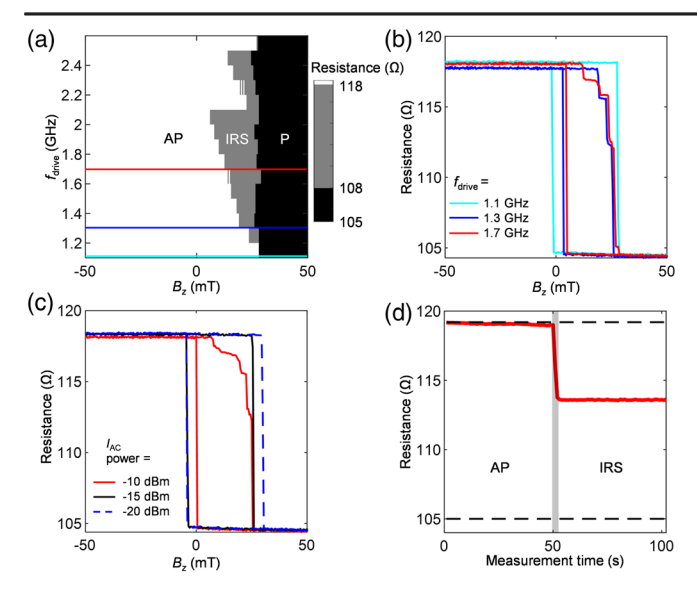


FIG. 2. (a) Inducing a transition to IRS in a 350 nm device by sweeping the magnetic field with the application of constant microwave current $I_{\rm ac}$. Field scan direction is from -50 to +50 mT. Colored lines are cuts shown in (b). (b) A cross-sectional view of (a) including the field sweep from negative to positive values to complete the hysteresis loop. (c) Microwave power dependence on AP \rightarrow IRS transition at fixed frequency $f_{\rm drive}=1.7$ GHz. (d) Stability of the IRS is demonstrated by applying a 1 sec $I_{\rm ac}$ burst (pulse applied in gray region) to transition from AP to IRS and allowing the free layer to reach static equilibrium. Static magnetic field was held at 20 mT and rf frequency $f_{\rm drive}=1.6$ GHz.

typically found to be most efficient when the microwave frequency matches a ferromagnetic resonance (FMR) mode of the free layer. As in the case with the pulse experiment, initializing the MTJ in the AP state and then briefly applying the microwave current in a one-second burst to induce the AP \rightarrow IRS transition shows that the IRS is a persistent state, rather than dynamically stabilized [Fig. 2(d)].

To characterize the dynamics of the MTJ in the ferromagnetic and intermediate resistance states, we perform homodyne-detected spin-transfer driven magnetic resonance measurements [28]. An amplitude-modulated $I_{\rm ac}$ is mixed with a small dc current bias $I_{\rm dc}$ through a bias tee and applied to the MTJ. The ac component of the MTJ response $V_{\rm ac}$ is measured on a lock-in amplifier locked to the modulation frequency. From the results with microwave-assisted nucleation, the AP → IRS transition is expected to occur naturally as a result of the resonant driving current. A key difference between the nucleation experiment and this setup is that now the frequency is swept from the lower limit to the upper limit while the field is held fixed, so that we obtain a spectrum for each magnetic field value. The lower panel of Fig. 3(a) shows the resonance spectrum of the 250 nm device with $I_{dc} = 20 \mu A$, as a function of B_z . At small fields on the left side of the graph,

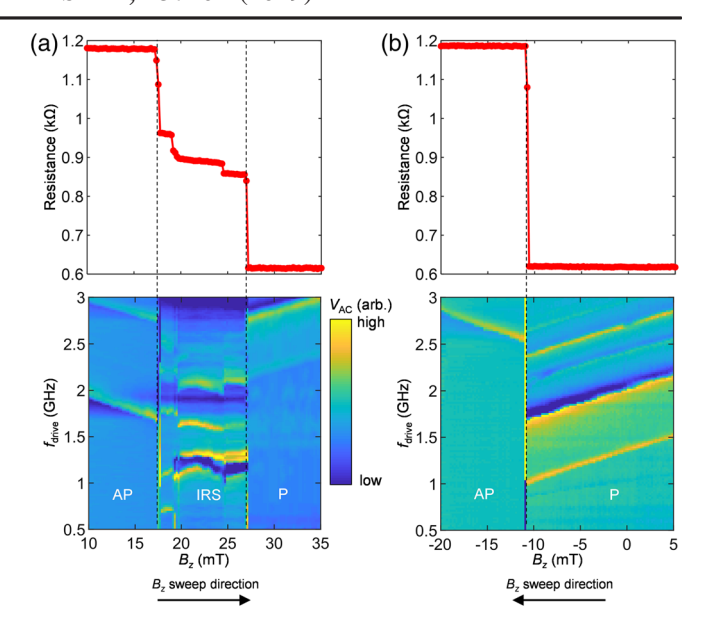


FIG. 3. Simultaneous measurement of dc resistance and magnetic resonance on the 250 nm MTJ when initialized in (a) the AP state and (b) the P state. The onset of the IRS at 17 mT in (a) is characterized by a new low-frequency mode at 1.2 GHz with a nonlinear dependence on field. In contrast, there is only a single discontinuity in the resonance spectrum representing the $P \rightarrow AP$ transition when initialized in P.

the MTJ is in the AP state and exhibits standard ferromagnetic resonance characterized by a linear dependence on external field and the appearance of higher-frequency spin-wave modes [29,30]. These modes have been shown to take the form of Bessel functions [31], and simulations of our devices show that they alternate between purely radial and purely azimuthal in nature [see Fig. 5(b)]. As the field is swept in the positive z direction, the microwave current induces domain nucleation and we see a discontinuity in the spectrum. While some modes appear to discretely shift, others seem to disappear entirely. At the same time, at least one new mode emerges at a lower frequency than the fundamental (uniform) ferromagnetic resonance. Increasing the field further leads to the disappearance of the low-frequency mode and the recovery of the Kittel-like FMR spectrum, now corresponding to the P state. Repeating the experiment while initialized in the P state and sweeping the field in the negative z direction shows a single discontinuity in the FMR spectrum, which is indicative of a simple transition between uniform ferromagnetic states [Fig. 3(b)].

Mixing the dc current with the driving ac current allows simultaneous measurement of the TMR during the resonance experiment (Fig. 3, upper panels). Although $I_{\rm dc}$ itself induces a shift in FMR frequencies, the shift is small enough that it doesn't qualitatively impact the spectra or any transitions. Recording the junction resistance during the FMR measurement confirms that the onset of the IRS exactly corresponds to the drastic change in spectrum.

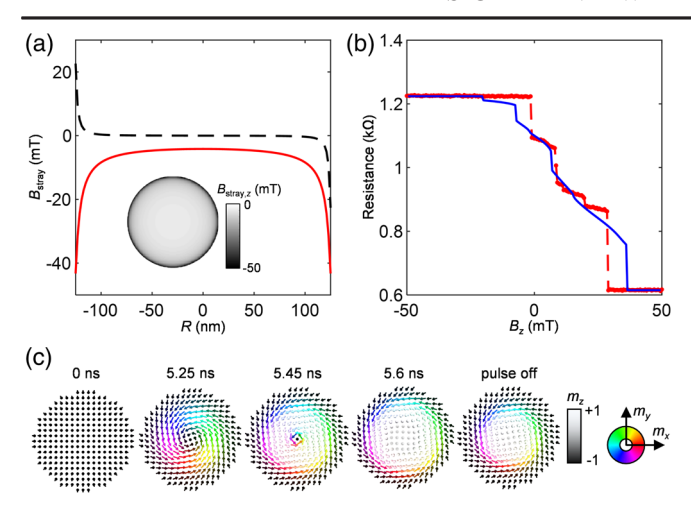


FIG. 4. (a) Simulated stray field z component (red) and x component (dotted black) seen by the free layer, along a diametric cut. Inset: spatial profile of the z component of the stray field. (b) Magnetic field dependence of the IRS (dotted red) and comparison with simulated skyrmion evolution with disorder (blue). The addition of magnetic disorder creates discontinuities in the magnetoresistance that match the observed behavior. (c) Snapshots of skyrmion formation via current pulse.

This result suggests that the IRS is a metastable, topologically nontrivial spin texture within the MTJ free layer.

To determine the nature of the nonferromagnetic IRS, we perform micromagnetic simulations of the free layer magnetization. We first compute the stray field from the magnetic layers near the free layer. Although the MTJs are designed to minimize the stray field's influence on the free layer, there may be significant torque near the nanopillar edge [32]. Simulations estimate that the free layer experiences a 50 mT out-of-plane field at the disk edge which quickly drops to less than 5 mT at the disk center. This stray field cants the spins at the edge of the disk and favors edge spins that are aligned with the stray field. The existence of this stray field is consistent with Fig. 1(b), as the MTJ displays a preference toward the antiparallel state (loop shifted in the positive B_z direction), indicating an overcompensated reference layer.

Next we simulate the behavior of the free layer when a current pulse or resonant microwave current is applied [Fig. 4(c)]. When the device is initialized in the AP state, a 10 ns current pulse exerts a torque that begins to rotate magnetic moments about a radial axis. However, the stray field makes edge spins more resistant to this rotation. Furthermore, there is no STT at the center of the disk where the spins are completely parallel to the spin polarization (in the z direction). This results in a ring of magnetic moments that experience the greatest net force from STT [second snapshot in Fig. 4(c)], and these are the first to reverse direction to form two concentric Bloch domain walls (third snapshot). The inner wall then collapses and the outer wall shrinks to form a single skyrmion (fourth and fifth snapshots). A calculation of the topological charge q of the final

state confirms that the skyrmion is very nearly quantized (q=0.996), see Supplemental Material [19]). Interestingly, the predicted skyrmion is of Bloch type rather than Néel type; this is consistent with the observation that Bloch domain walls are energetically favorable over Néel walls in ferromagnetic thin films with PMA and vanishing DMI [33]. We expect the DMI to be negligible in our devices, since the free layer is sandwiched between MgO layers. The symmetry of the adjacent materials mostly cancels out any small DMI that could arise from the MgO/CoFeB interface [34]. Simulating the free layer in the presence of a persistent microwave current tuned to match ferromagnetic resonance shows a qualitatively similar skyrmion transition.

The magnetic field dependence of the IRS in experiments is also consistent with the skyrmion picture. As the field is swept through the IRS, the initially small skyrmion (estimated to be 75 nm in diameter at its smallest, near zero field) grows larger and the average M_z is reduced. This leads to a decrease in resistance, until the skyrmion expands to the boundary of the disk and turns into the P state. Simulations of a skyrmion evolving in this way are consistent with the observed TMR curve [Fig. 1(d)], with one discrepancy: measurements show discrete steps in the magnetoresistance curve. When magnetic disorder is incorporated into the simulation, the magnetoresistance curve acquires steps similar to the observed behavior [Fig. 4(b), see Supplemental Material [19] for details] [35].

The dynamics of the skyrmion can be experimentally inferred from the IRS resonance spectrum. At IRS onset, the ferromagnetic resonance modes vanish and a large negative peak appears near 1 GHz. Simulations based on material parameters extracted from FMR identify this mode as the breathing mode, or expansion and contraction of the skyrmion [Figs. 5(a), 5(b)]. The breathing mode is a ubiquitous characteristic of skyrmions and has a complex dependence on external fields [18]. If the skyrmion core is aligned with the reference layer, as is the case in these devices, then a positive (negative) current causes skyrmion expansion (contraction) and consequently a negative peak in the spectrum. In further contrast with ferromagnetic resonance lines, which show substantial asymmetry due to the current-induced fieldlike torque, the skyrmion breathing mode is mostly symmetric [Figs. 5(c), 5(d)]. Simulations of the resonant frequency profile agree well with the observed profiles [Figs. 5(c), 5(d) insets].

The MTJ can be a powerful tool to create and sense skyrmions in magnetic films. Our results show that a single skyrmion with a diameter smaller than 100 nm can cause a change in junction resistance of almost 10%, which is more than sufficient for electrical detection. We can also conclude that the energy cost for current-induced skyrmion creation is less than the energy of full ferromagnetic switching since the transition to a skyrmion state occurs at lower applied field in pulse experiments.

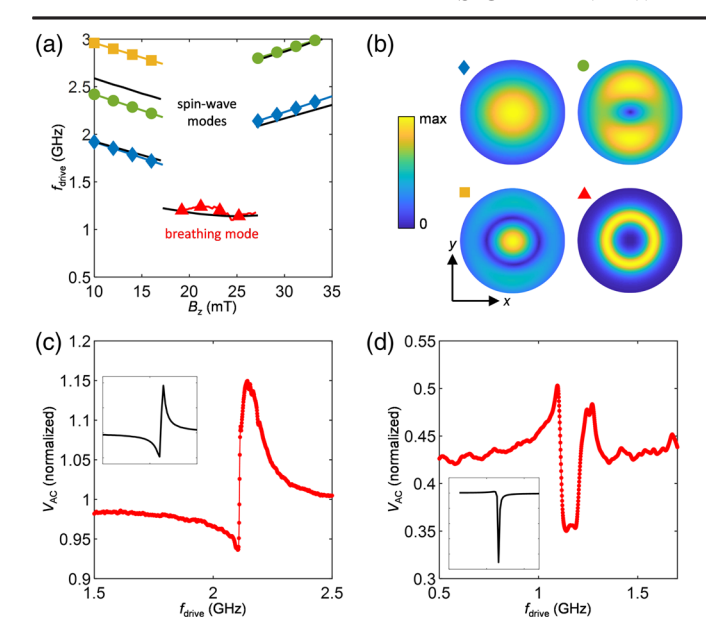


FIG. 5. (a) The magnetic resonance landscape of the 250 nm device from Fig. 3 (colored symbols) and comparison to simulations (solid black lines). (b) Corresponding spatial profiles of ferromagnetic spin-wave mode amplitudes showing alternating radial (blue diamonds, yellow squares) and azimuthal (green circles) modes. Also shown is the skyrmion breathing mode (red triangles). Profiles for the FM (skyrmion) states were obtained from the Fourier transform of m_x (m_z) dynamics for each cell in the simulation. (c) Frequency profile of the first FMR mode taken at 5 mT in the AP state. (d) Frequency profile of the skyrmion breathing mode taken at 20 mT. Insets are simulated profiles.

Unlike the prevailing imaging techniques, pure electrical detection only provides indirect evidence of a skyrmion state. It is therefore critical that the magnetoresistance and the magnetic resonance spectrum are mutually consistent to discriminate skyrmions from other spin textures. As demonstrated in the Supplemental Material Fig. S3 [19], the magnetoresistance curve of a single skyrmion is qualitatively similar to the magnetoresistance that would arise from the formation of a generic magnetic bubble. However, the skyrmion breathing mode frequency is expected to be an order of magnitude higher than the fundamental mode of a bubble, which emphasizes the need for resonance measurements. In addition to theoretical considerations, our experimental observations are qualitatively distinct from other published work on domains and defects in magnetic nanostructures [36,37].

To conclude, we have experimentally demonstrated the deterministic electrical switching of a MTJ free layer from a ferromagnetic state to a nontrivial spin texture. Micromagnetic simulations, using our device parameters, strongly suggest that this texture is a single skyrmion created in the free layer, facilitated by the reference layer stray field that favors spins at the pillar edge to be canted away from the bulk magnetization. This work could lead to purely electrical creation, detection, and characterization

of skyrmions in MTJs for memory and computational applications.

This work was supported by Functional Accelerated nanoMaterial Engineering (FAME), a STARnet center and the NSF under Grant No. DMR-1809155.

- *Corresponding author. jiangh@physics.ucla.edu
- [1] A. Fert, N. Reyren, and V. Cros, Magnetic skyrmions: Advances in physics and potential applications, Nat. Rev. Mater. **2**, 17031 (2017).
- [2] X. Zhang, M. Ezawa, and Y. Zhou, Magnetic skyrmion logic gates: Conversion, duplication and merging of skyrmions, Sci. Rep. 5, 9400 (2015).
- [3] Y. Huang, W. Kang, X. Zhang, Y. Zhou, and W. Zhao, Magnetic skyrmion-based synaptic devices, Nanotechnology 28, 08LT02 (2017).
- [4] G. Yang, P. Stano, J. Klinovaja, and D. Loss, Majorana bound states in magnetic skyrmions, Phys. Rev. B 93, 224505 (2016).
- [5] W. Koshibae, Y. Naneko, J. Iwasaki, M. Kawasaki, Y. Tokura, and N. Nagaosa, Memory functions of magnetic skyrmions, Jpn. J. Appl. Phys. 54, 053001 (2015).
- [6] W. Kang, Y. Huang, C. Zheng, W. Lv, N. Lei, Y. Zhang, X. Zhang, Y. Zhou, and W. Zhou, Voltage controlled magnetic skyrmion motion for racetrack memory, Sci. Rep. 6, 23164 (2016).
- [7] D. Bhattacharya, M. M. Al-Rashid, and J. Atulasimha, Voltage controlled core reversal of fixed magnetic skyrmions without a magnetic field, Sci. Rep. 6, 31272 (2016).
- [8] S. Pollard, J. Garlow, J. Yu, Z. Wang, Y. Zhu, and H. Yang, Observation of stable Neel skyrmions in cobalt/palladium multilayers with Lorentz transmission electron microscopy, Nat. Commun. 8, 14761 (2017).
- [9] Y. Onose, Y. Okamura, S. Seki, S. Ishiwata, and Y. Tokura, Observation of magnetic excitations of skyrmion crystal in a helimagnetic insulator Cu₂OSeO₃, Phys. Rev. Lett. 109, 037603 (2012).
- [10] M. Schott, A. Bernand-Mantel, L. Ranno, S. Pizzini, J. Vogel, H. Bea, C. Baraduc, S. Auffret, G. Gaudin, and D. Givord, The skyrmion switch: turning magnetic skyrmion bubbles on and off with an electric field, Nano Lett. 17, 3006 (2017).
- [11] A. Bogdanov and U. Rößler, Chiral symmetry breaking in magnetic thin films and multilayers, Phys. Rev. Lett. 87, 037203 (2001).
- [12] O. Boulle, J. Vogel, H. Yang, S. Pizzini, D. d. S. Chavez, A. Locatelli, T. O. Mentes, A. Sala, L. Buda-Prejbeanu, O. Klein, M. Belmeguenai, Y. Roussigne, A. Stashkevich, S. M. Cherif, L. Aballe, M. Foerster, M. Chshiev, S. Auffret, I. M. Miron, and G. Gaudin, Room-temperature chiral magnetic skyrmions in ultrathin magnetic nanostructures, Nat. Nanotechnol. 11, 449 (2016).
- [13] Y. Dai, H. Wang, P. Tao, T. Yang, W. Ren, and Z. Zhang, Skyrmion ground state and gyration of skyrmions in magnetic nanodisks without the Dzyaloshinsky-Moriya interaction, Phys. Rev. B 88, 054403 (2013).

- [14] K. Guslienko, Skyrmion state stability in magnetic nanodots with perpendicular anisotropy, IEEE Magn. Lett. 6, 1 (2015).
- [15] T. Devolder, A. L. Goff, and V. Nikitin, Size dependence of nanosecond-scale spin-torque switching in perpendicularly magnetized magnetic tunnel junctions, Phys. Rev. B. 93, 224432 (2016).
- [16] J. Sampaio, V. Cros, S. Rohart, A. Thiaville, and A. Fert, Nucleation, stability, and current-induced motion of isolated magnetic skyrmions in nanostructures, Nat. Nanotechnol. 8, 839 (2013).
- [17] Y. Nakatani, M. Hayashi, S. Kanai, S. Fukami, and H. Ohno, Electric field control of skyrmions in magnetic nanodisks, Appl. Phys. Lett. **108**, 152403 (2016).
- [18] J.-V. Kim, F. Garcia-Sanchez, J. Sampaio, C. Moreau-Luchaire, V. Cros, and A. Fert, Breathing modes of confined skyrmions in ultrathin magnetic dots, Phys. Rev. B 90, 064410 (2014).
- [19] See Supplemental Material at http://link.aps.org/ supplemental/10.1103/PhysRevLett.122.257201 for MTJ stack details, data on additional devices, and simulation methods, etc., which includes Refs. [20–23].
- [20] A. Vansteenkiste, J. Laliaert, M. Dvornik, M. Helsen, F. Garcia-Sanchez, and B. V. Waeyenberge, The design and verification of MuMax3, AIP Adv. 4, 107133 (2014).
- [21] S. Heinz, K. v. Bergmann, M. Menzel, J. Brede, A. Kubetzka, R. Weisendanger, G. Bihlmayer, and S. Blugel, Spontaneous atomic-scale magnetic skyrmion lattice in two dimensions, Nat. Phys. 7, 713 (2011).
- [22] S. M. Mohseni, S. R. Sani, J. Persson, T. N. A. Nguyen, S. Chung, Y. Pogoryelov, P. K. Muduli, E. Iacocca, A. Eklund, R. K. Dumas, S. Bonetti, A. Deac, M. A. Hoefer, and J. Akerman, Spin torque-generated magnetic droplet solitons, Science 339, 1295 (2013).
- [23] X. Zhang, W. Cai, X. Zhang, Z. Wang, Z. Li, Y. Zhang, K. Cao, N. Lei, W. Kang, Y. Zhang, H. Yu, Y. Zhou, and W. Zhou, Skyrmions in magnetic tunnel junctions, ACS Appl. Mater. Interfaces 10, 16887 (2018).
- [24] S. Parkin, N. More, and K. Roche, Oscillations in exchange coupling and magnetoresistance in metallic superlattice structures: Co/Ru, Co/Cr, and Fe/Cr, Phys. Rev. Lett. 64, 2304 (1990).
- [25] H. Gan, R. Malmhall, Z. Wang, B. K. Yen, J. Zhang, X. Wang, Y. Zhou, X. Hao, D. Jung, K. Satoh, and Y. Huai, Perpendicular magnetic tunnel junction with thin CoFeB/Ta/Co/Pd/Co reference layer, Appl. Phys. Lett. 105, 192403 (2014).
- [26] S. Ikeda, K. Miura, H. Yamamoto, K. Mizunuma, H. Gan, M. Endo, S. Kanai, J. Hayakawa, F. Matsukura, and H. Ohno, A perpendicular-anisotropy CoFeB-MgO magnetic tunnel junction, Nat. Mater. 9, 721 (2010).
- [27] H. Suto, T. Nagasawa, K. Kudo, K. Mizushima, and R. Sato, Microwave-assisted switching of a single perpendicular

- magnetic tunnel junction nanodot, Appl. Phys. Express 8, 023001 (2015).
- [28] J. Sankey, P. Braganca, A. Garcia, I. Krivorotov, R. Buhrman, and D. Ralph, Spin-transfer-driven ferromagnetic resonance of individual nanomagnets, Phys. Rev. Lett. 96, 227601 (2006).
- [29] A. Helmer, S. Cornelissen, T. Devolder, J.-V. Kim, W. v. Roy, L. Lagae, and C. Chappert, Quantized spin-wave modes in magnetic tunnel junction nanopillars, Phys. Rev. B 81, 094416 (2010).
- [30] Z. Zeng, K. Cheung, H. W. Jiang, I. Krivorotov, J. Katine, V. Tiberkevich, and A. Slavin, Evolution of spin-wave modes in magnetic tunnel junction nanopillars, Phys. Rev. B 82, 100410 (2010).
- [31] V. Naletov, G. d. Loubens, G. Albuquerque, S. Borlenghi, V. Cros, G. Faini, J. Grollier, H. Hurdequint, N. Locatelli, B. Pigeau, A. Slavin, V. Tiberkevich, C. Ulysse, T. Valet, and O. Klein, Identification and selection rules of the spin-wave eigenmodes in a normally magnetized nanopillar, Phys. Rev. B 84, 224423 (2011).
- [32] D. Gopman, D. Bedau, S. Mangin, C. Lambert, E. Fullerton, J. Katine, and A. Kent, Asymmetric switching behavior in perpendicularly magnetized spin-valve nanopillars due to the polarizer dipole field, Appl. Phys. Lett. 100, 062404 (2012).
- [33] M. Benitez, A. Hrabec, A. Mihai, T. Moore, G. Burnell, D. McGrouther, C. Marrows, and S. McVitie, Magnetic microscopy and topological stability of homochiral Neel domain walls in a Pt/Co/AlOx trilayer, Nat. Commun. 6, 8957 (2015).
- [34] C. Moreau-Luchaire, C. Moutafis, N. Reyren, J. Sampaio, C. A. F. Vaz, N. V. Horne, K. Bouzehouane, K. Garcia, C. Deranlot, P. Warnicke, P. Wohlhuter, J.-M. George, M. Weigand, J. Raabe, V. Cros, and A. Fert, Additive chiral interfacial interaction in multilayers for stabilization of small individual skyrmions at room temperature, Nat. Nanotechnol. 11, 444 (2016).
- [35] R. Juge, S.-G. Je, D. d. S. Chavez, S. Pizzini, L. Buda-Prejbeanu, L. Aballe, M. Foerster, A. Locatelli, T. Mentes, A. Sala, F. Macherozzi, S. Dhesi, S. Auffret, E. Gautier, G. Gaudin, J. Vogel, and O. Boulle, Magnetic skyrmions in confined geometries: effect of the magnetic field and the disorder, J. Magn. Magn. Mater. 455, 3 (2018).
- [36] S. Ingvarsson, G. Xiao, S. S. P. Parkin, W. J. Gallagher, G. Grinstein, and R. H. Koch, Low-frequency magnetic noise in micron-scale magnetic tunnel junctions, Phys. Rev. Lett. **85**, 3289 (2000).
- [37] D. Ravelosona, S. Mangin, Y. Lemaho, J. A. Katine, B. D. Terris, and E. E. Fullerton, Domain wall creation in nanostructures driven by a spin-polarized current, Phys. Rev. Lett. **96**, 186604 (2006).

Supplementary: Experimental Observation of Single Skyrmion Signatures in a Magnetic Tunnel Junction

N. E. Penthorn¹, X. Hao², Z. Wang², Y. Huai², and H. W. Jiang^{1*}

1. MTJ fabrication methods

The MTJ stack was deposited via magnetron sputtering with an Anelva NC7900 MRAM PVD system. In addition to the main MgO tunneling barrier, there is a second MgO barrier directly above the free layer that gives the free layer additional perpendicular magnetic anisotropy. The main barrier has a resistance-area product of $10~\Omega~\mu m^2$, while the second barrier has a resistance-area product of less than $0.5~\Omega~\mu m^2$. The full structure cross-section is shown in Fig. S1.

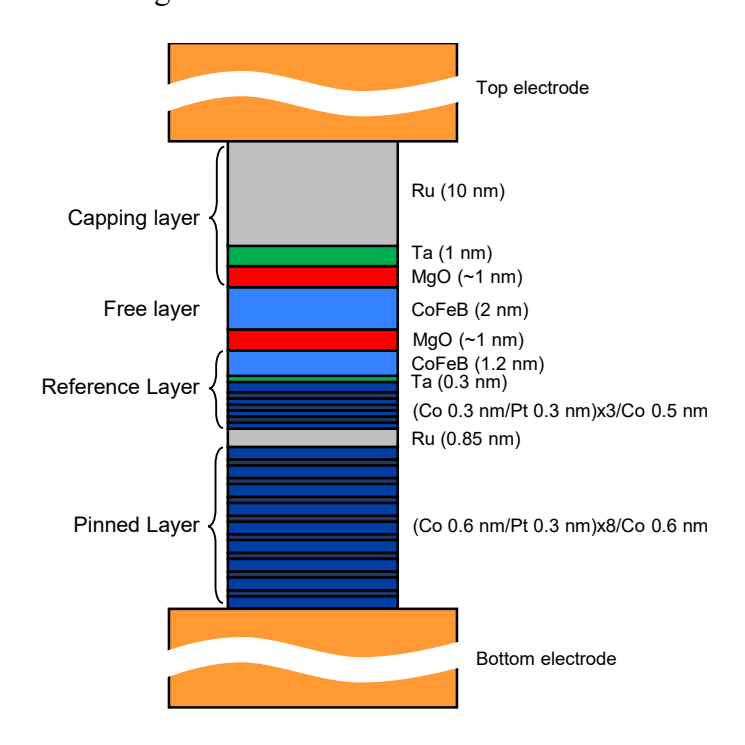


FIG. S1. MTJ layer cross-section.

¹Department of Physics & Astronomy, University of California, Los Angeles, California 90095, USA

²Avalanche Technology, Fremont, California 95438, USA

2. Micromagnetic simulations

Simulations were performed with the GPU-accelerated micromagnet simulation program MuMax³ [1]. The device geometry was treated as a single 2 nm-thick nanodisk under the influence of STT from a fixed polarizer and discretized the disk into a mesh of 128×128×1 cells. The stray field was added as a static vector field, using the simulated field of Fig. 4a in the main text. Magnetization dynamics in MuMax³ are computed from the Landau-Lifshitz-Gilbert equation:

$$\frac{\partial \mathbf{m}}{\partial t} = \frac{-\gamma}{1 + \alpha^2} \left[\mathbf{m} \times \mathbf{H}_{\text{eff}} + \alpha \left(\mathbf{m} \times (\mathbf{m} \times \mathbf{H}_{\text{eff}}) \right) \right]$$
(S1)

where m is the reduced magnetization, γ is the gyromagnetic ratio, α is the Gilbert damping coefficient, and $H_{\rm eff}$ is the effective magnetic field which comprises effective fields due to demagnetization, perpendicular anisotropy, and Heisenberg exchange. STT effects were simulated with the addition of Slonczewski spin-torque terms to the LLG equation:

$$\tau_{\rm SL} = \frac{j_z \hbar}{M_{\rm s} e d} \left[\frac{\epsilon - \alpha \epsilon'}{1 + \alpha^2} (\boldsymbol{m} \times (\boldsymbol{p} \times \boldsymbol{m})) - \frac{\epsilon' - \alpha \epsilon}{1 + \alpha^2} \boldsymbol{m} \times \boldsymbol{p} \right]$$
(S2)

where j is the current density, M_s is the saturation magnetization, d is the disk thickness, p is the fixed layer magnetization, and ϵ and ϵ' are spin-torque parameters detailed in ref. [1]. To convert magnetization to resistance, the MTJ conductance was assumed to depend linearly on the projection of m onto p. The resistance as a function of volume-averaged magnetization is then given by

$$\frac{1}{R(\boldsymbol{m})} = \frac{1}{2} \left(\frac{1}{R_{\rm P}} + \frac{1}{R_{\rm AP}} \right) + \frac{1}{2} \left(\frac{1}{R_{\rm P}} - \frac{1}{R_{\rm AP}} \right) \langle m_z \rangle \tag{S3}$$

where $R_P(R_{AP})$ is the resistance in the parallel (antiparallel) state.

Parameters used in simulations are enumerated in Table 1.

TABLE 1. Relevant simulation parameters used in main text.

Parameter	value
Saturation magnetization $(\mu_0 M_s)$	1.6 T
Exchange constant (A_{ex})	$20 \times 10^{-12} \text{ J/m}$
Perpendicular anisotropy constant ($K_{\rm u}$) 1.011 × 10 ⁶ J/m ³
Gilbert damping parameter (α)	0.01
Dzyaloshinskii-Moriya interaction t	erm 0 J/m^2
Ref. layer spin polarization (P)	0.6
Slonczewski spin-torque parameter	(Λ) 1
Secondary spin-torque parameter (ϵ	') 0.1
Free layer thickness	2 nm

The stray field was treated as originating from an overcompensated reference layer, since the hysteresis loop in the absence of excitations was shifted in favor of the AP state (figure 1b in the main text). It is recreated in simulations by creating a disk of magnetic moments with the same radius and material parameters as the free layer and fixing the magnetization to be pointing in the -z direction. The total field above this disk at a distance of 0.8 nm is considered to be the stray field experienced by the free layer. The amount of screening due to other magnetic layers, such as the reference layer, is wrapped into a scaling factor that acts as a free parameter of the stray field and is adjusted to match the hysteresis loop. For the 250 nm device, the stray field is reduced by half as a result of screening.

Skyrmion creation due to a current pulse was simulated by initializing in the AP state ($M_z = -1$), adding the stray field as a static external magnetic field, and turning on a fixed current density of 8.66×10^9 A/m² for 10 ns. During the pulse the Oersted field of the current was also added as an external magnetic field, with the assumption that the

current density is uniform throughout the free layer. Skyrmion creation due to a microwave current was simulated in much the same way, with the stray field and current-induced Oersted field incorporated.

Magnetic resonance was simulated by applying a current pulse (and its induced Oersted field) to the free layer in the form of a cardinal sine wave, $I(t) = I_{AC} \sin(2\pi f_c t)/(2\pi f_c t)$ with $I_{AC} = 0.5$ mA. This pulse has uniform spectral density in all frequencies below the cutoff frequency f_c . The m_z free layer component was measured as a function of time in the presence of the pulse for 50 ns and a power spectral density was constructed from the time domain data up to $f_c = 10$ GHz. This was repeated for each magnetic field value. To achieve sharp spectral peaks, the Gilbert damping parameter was set to $\alpha = 0.001$ in the resonance simulations.

The spatial profiles of the magnetic resonance modes were simulated using the stroboscopic method described in reference [2]. From the simulated spectrum, a mode is chosen and a sinusoidal current is applied at resonance. The free layer magnetization is allowed to evolve for 20 periods of oscillation, then the magnetization of each simulation cell is recorded over 10 more periods with 25 data points per period. For each cell, the 10 periods of time evolution are averaged together. The averaging removes any motion of the magnetization that is non-resonant with the AC drive. Finally the Fourier transform is calculated for each magnetic moment to obtain oscillation amplitudes at the resonant frequency as a function of position in real space.

Disorder can be incorporated into the simulation model by breaking the geometry into grain regions with an average grain size r_{grain} and assigning each grain a value of PMA that follows a normal distribution centered at the measured coefficient value K_0 . The grains

were randomly generated using the Voronoi tessellation method. Setting $r_{\text{grain}} = 10 \text{ nm}$ and allowing fluctuations of the PMA coefficient to be $\pm 5\%$ of K_0 , the simulated magnetoresistance curve acquires discretized steps (see Fig. 4b in main text).

3. Additional Data from a 400nm MTJ

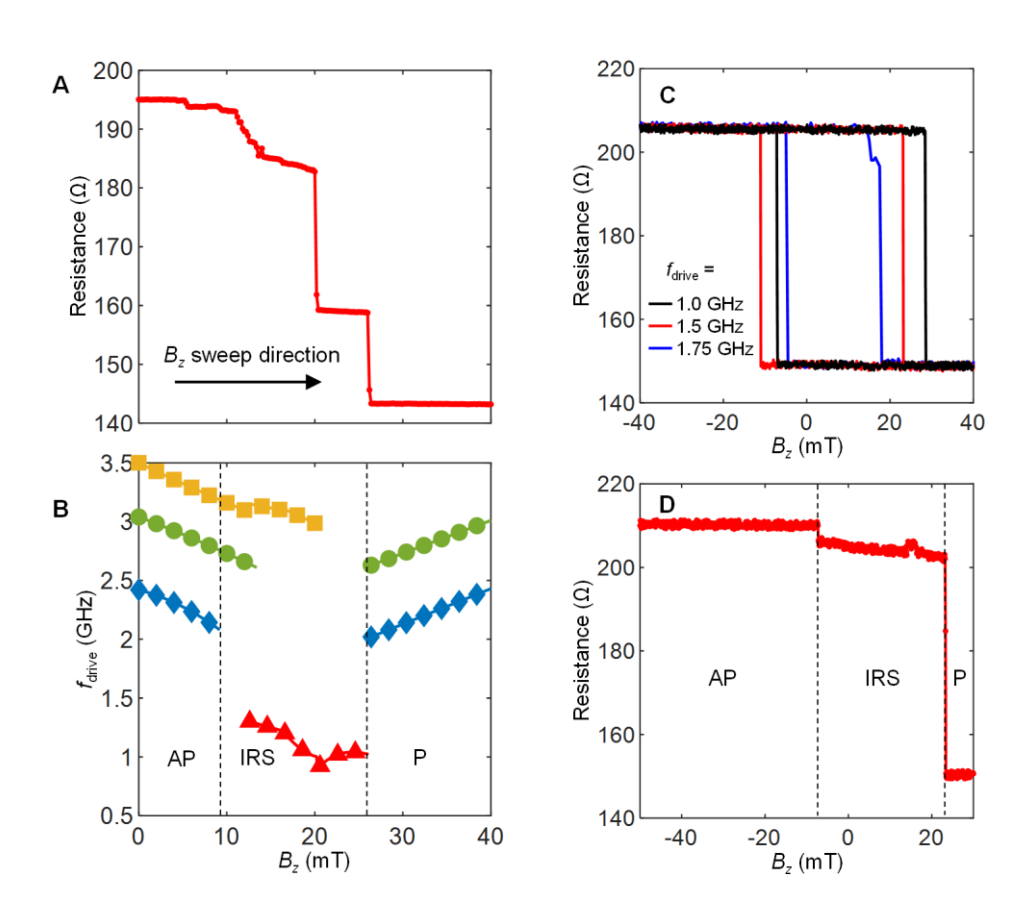


FIG. S2. Data from a 400 nm diameter MTJ. (a), (b) FMR and junction resistance. At the onset of the IRS, some ferromagnetic resonance modes disappear and others are only slightly shifted. Visible higher-frequency modes seem to persist even when the measured resistance differs greatly from either the P or AP state, indicating that these modes are not suppressed by the presence of a node at the free layer center, i.e. a skyrmion. (c) Microwave-excited nucleation of the IRS at 1.75 GHz and comparison to off-resonance RH loops. (d) Magnetoresistance curve showing field dependence of the IRS with no current excitation. IRS was nucleated with a 1.75 GHz microwave current at 14 mT and the field was swept in both directions with the microwave current off.

4. Topological charge and bubble state

The topological charge q of the skyrmion can be numerically computed as [3]

$$q = \frac{1}{4\pi} \int \boldsymbol{m} \cdot (\partial_x \boldsymbol{m} \times \partial_y \boldsymbol{m}) dx dy$$
 (S4)

where m is the reduced magnetization of each simulation cell. For a skyrmion in the 250 nm device presented in this study, q is found to range from 0.992 to 0.996. Any small deviation from the quantized values of $q = \pm 1$ are a result of the discretized nature of the micromagnetic simulation and the finite geometry.

To distinguish the topologically nontrivial skyrmion from a generic region of flipped magnetic spins, simulations identify a metastable bubble state that displays a similar magnetoresistance curve to the skyrmion but is topologically trivial with q = -0.009 (Fig. S3a). In this case, the bubble state creates an IRS that evolves in much the same way with applied field (Fig. S3c) but has a characteristic resonant frequency that is an order of magnitude lower than all resonances seen in experiments (< 100 MHz). The bubble resonance is characterized by uniform, in-phase precession of the domain wall spins and appears to be proportional to the in-plane magnetic anisotropy [4]. Since the in-plane anisotropy of our devices is negligible, we can conclude that the bubble resonant frequency would be close to zero. This highlights the importance of measuring the breathing mode frequency in concurrence with the DC magnetoresistance curve to positively identify skyrmion states.

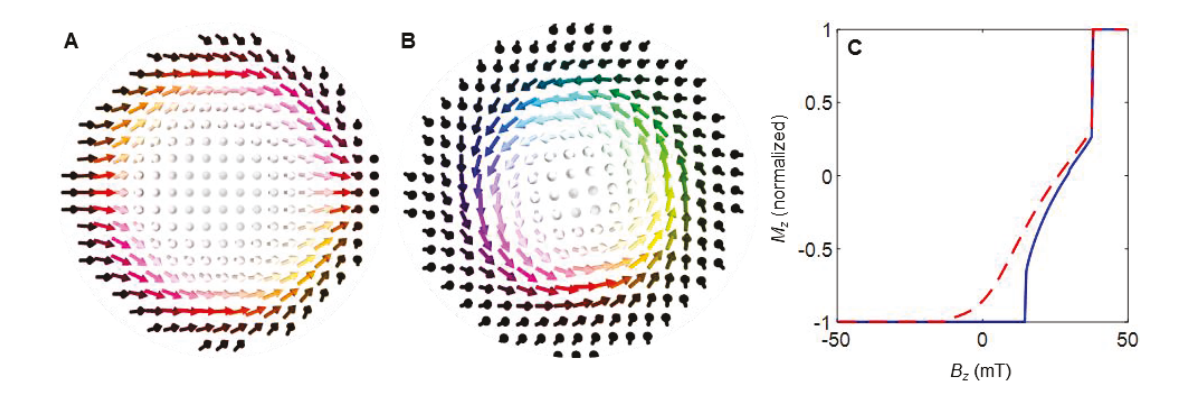


FIG. S3. Comparison between skyrmion and topologically trivial bubble. (a) Simulated bubble state. Similar to the skyrmion spin configuration (b), the bubble is described by a circular region of flipped spins. Unlike the skyrmion, the bubble domain wall has a net magnetic moment in the x direction. The bubble was found to have a topological charge close to zero, making it topologically equivalent to the uniform ferromagnetic state. (c) Out-of-plane free layer magnetization m_z as a function of field, in the presence of a skyrmion (dotted red line) or a bubble (blue line). The magnetoresistance curves in the two cases are quite similar, which demonstrates that magnetoresistance alone is not sufficient to identify skyrmion states.

5. Role of temperature in skyrmion creation and detection

We found that temperature played a critical role in facilitating skyrmion formation. Relying only on the MTJ geometry, saturation magnetization and magnetic anisotropy to stabilize the skyrmion can cause the energy barrier between ferromagnetic and skyrmion states to be quite small, leading to high susceptibility to thermal perturbations. Additionally, cryogenic temperatures cause an increase in interfacial perpendicular magnetic anisotropy. Because the free layer tilts in-plane at higher temperatures from reduced anisotropy, it is impossible to discriminate the magnetoresistance curve of the skyrmion-induced IRS from standard in-plane ferromagnetism. The full temperature dependence of skyrmions in MTJs deserves further study.

6. Differentiating the nucleation mechanism from existing computational studies

The nucleation mechanism proposed in this work differs from the one described in [5], where magnetic moments at the free layer edge flip first and the domain wall collapses inward to form a skyrmion. In our system, nucleation relies on large-amplitude coherent precession of magnetic moments away from the edge. If the reference layer was the only contributor to the stray field, then we would expect skyrmion nucleation during the $P\rightarrow AP$ transition. However, due to overcompensation of the reference layer, the stray field at the edge points along -z and favors the AP configuration. This leads to the observed $AP\rightarrow P$ nucleation despite the fundamentally different dynamics.

References

- [1] A. Vansteenkiste, J. Laliaert, M. Dvornik, M. Helsen, F. Garcia-Sanchez and B. V. Waeyenberge, "The design and verification of MuMax3," *AIP Advances*, vol. 4, 107133, (2014).
- [2] J.-V. Kim, F. Garcia-Sanchez, J. Sampaio, C. Moreau-Luchaire, V. Cros and A. Fert, "Breathing modes of confined skyrmions in ultrathin magnetic dots," *Phys. Rev. B*, vol. 90, 064410, (2014).
- [3] S. Heinz, K. v. Bergmann, M. Menzel, J. Brede, A. Kubetzka, R. Weisendanger, G. Bihlmayer and S. Blugel, "Spontaneous atomic-scale magnetic skyrmion lattice in two dimensions," *Nat. Phys.*, vol. 7, 713-718, (2011).
- [4] S. M. Mohseni, S. R. Sani, J. Persson, T. N. A. Nguyen, S. Chung, Y. Pogoryelov, P. K. Muduli, E. Iacocca, A. Eklund, R. K. Dumas, S. Bonetti, A. Deac, M. A. Hoefer and J. Akerman, "Spin torquegenerated magnetic droplet solitons," *Science*, vol. 339, 1295-1298, (2013).
- [5] X. Zhang, W. Cai, X. Zhang, Z. Wang, Z. Li, Y. Zhang, K. Cao, N. Lei, W. Kang, Y. Zhang, H. Yu, Y. Zhou and W. Zhou, "Skyrmions in magnetic tunnel junctions," *ACS Appl. Mater. Interfaces*, vol. 10, 16887-16892, (2018).